PHYSICAL REVIEW C
NUCLEAR PHYSICS

THIRD SERIES, VOLUME 32, NUMBER 1 JULY 1985

Hermitian folded-diagram potentials in nucleon-nucleon scattering

K. Holinde* and Mikkel B. Johnson
Los Alamos National Laboratory, Los Alamos, New Mexico 87545

R. Machleidt*
TRIUMF, Vancouver, British Columbia, Canada V6T 2A3
(Received 6 February 1985)

We assess the adequacy of folded diagrams as a practical method for determining a Hermitian, instantaneous potential derived from meson exchange. The nucleon-nucleon scattering amplitude calculated from this folded-diagram potential agrees quite favorably with model-exact results. We compare our results to those based on a recently proposed non-Hermitian folded-diagram description.

I. INTRODUCTION

A formal development arising from studies of the nuclear shell model showed how effective interactions and effective operators acting within a restricted "model space" could be calculated from a more fundamental description acting in a larger Hilbert space. According to these theories, the quantum mechanics in the model space would yield some of the important observable consequences of the more exact theory and possibly simplify the solution of the many-body problem. The particular version of this procedure known as folded diagrams showed how the goal could be accomplished in terms of an energy-independent effective interaction, i.e., a potential. The theory of folded diagrams comes in a version leading to non-Hermitian[1-3] and Hermitian[4] forms for the relevant operators in the model space.

An application of folded diagrams to calculate a Hermitian nucleon-nucleon interaction was made in Ref. 5. An instantaneous, Hermitian potential has many advantages in nuclear physics. Absence of energy dependence is useful because there are fewer variables to carry through calculations in many-body systems. The symmetry built into the effective interaction $\overline{H}$ by virtue of its Hermiticity is desirable because the eigenstates of the Hamiltonian are then orthonormal and the eigenvalues are guaranteed to be real.

The theory of Ref. 5 addressed the solution to the following problem. Suppose that H is the exact Hamiltonian in the full Hilbert space written in terms of nucleons and mesons, and $\{\theta_i\}$ is a set of observables. Let the corresponding quantities in the model space of nucleons only be $\overline{H}$ and $\{\overline{\theta}_i\}$. Furthermore, suppose that H and $\overline{H}$ have eigenstates

$$H\,|\,\psi_i\,\rangle = E_i\,|\,\psi_i\,\rangle \tag{1}$$

and

$$\overline{H}\,|\,\overline{\psi}_i\,\rangle = E_i\,|\,\overline{\psi}_i\,\rangle\ . \tag{2}$$

Reference 5 shows how to calculate a Hermitian $\overline{H}$ such that $|\,\psi_i\,\rangle$ and $|\,\overline{\psi}_i\,\rangle$ have the same phase shifts for nucleon-nucleon scattering below the meson-production threshold and the set $\{\overline{\theta}_i\}$ such that

$$\langle\,\psi_i\,|\,\theta_j\,|\,\psi_k\,\rangle = \langle\,\overline{\psi}_i\,|\,\overline{\theta}_j\,|\,\overline{\psi}_k\,\rangle\ . \tag{3}$$

The equality in Eq. (3) permits calculation of other properties of the system commonly regarded as probing off-shell information. Extension to the bound state would enable, for example, calculation of magnetic moments and form factors, in which case $\{\overline{\theta}_i\}$ would include the familiar exchange currents and folded-diagram corrections to them.

The solution to this problem expresses the interaction $\overline{H}$ and the operators $\{\overline{\theta}_i\}$ as an infinite series of terms. Retardation effects are accounted for by folded diagrams rather than an explicit energy dependence common in many familiar alternative descriptions. It was shown in Ref. 5 that the solution to this problem is not unique and that there is an infinite class of prescriptions leading to effective interactions and operators having the same observable consequences. The formal theory gives no reason to prefer one prescription over another. Because all prescriptions are physically equivalent, the only meaningful criterion for choosing one over another is the rate of convergence of its expansion. It was shown that the diagrammatic expansion for one (called $J1$ below) was simpler than all others, and it was singled out for this reason as possibly converging faster.

More recently a non-Hermitian prescription for the nucleon-nucleon interaction was advocated.[6] It was shown in this paper that the non-Hermitian potential preserved in principle the half-off-shell nucleon-nucleon T matrix

$$\langle \mathbf{p}' \mid T(p_0=p) \mid \mathbf{p} \rangle \ . \tag{4}$$

Because of this property, it was argued that the non-Hermitian potential should be preferred for practical calculations. Numerical comparisons to the Bonn[7] one-boson-exchange potential (OBEP) were made in Ref. 8 to assess the importance of the folded diagrams, and it was shown that the non-Hermitian potential gave a good reproduction of the phase shifts.

The purpose of the present paper is to show how well the Hermitian folded-diagram potential works in practice and to evaluate the relative advantage of the Hermitian and non-Hermitian results. In Sec. II we define the "model exact" problem to which we can compare the folded-diagram results and assess the rate of convergence of the expansion. Results are given in Sec. III, and our conclusion is presented in Sec. IV.

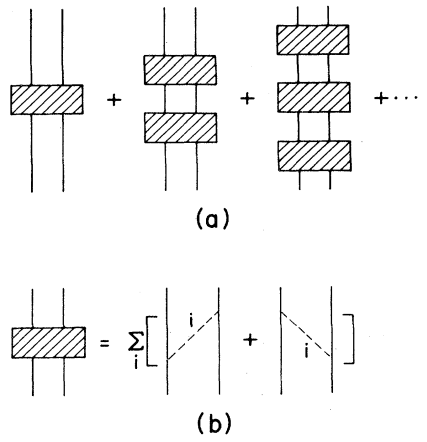

FIG. 1. Illustrating the terms included in the T matrix for the Bonn OBEP. (a) Expansion for the T matrix in terms of the quasipotential V, represented by a filled box. (b) Expression for V in the OBE approximation.

II. THEORY

In order to test the theory of Ref. 5, one would like to have an exactly solvable field theory. In the absence of a realistic field theoretical model of the nucleon-nucleon interaction that is exactly solvable, we will utilize the one-boson-exchange model of the Bonn group.[7] They select a particular subset of diagrams expected to be important and sum these to obtain the nucleon-nucleon scattering amplitude and deuteron properties. We will calculate a Hermitian folded-diagram potential based on this selection of diagrams and compare the scattering amplitude to that of the Bonn group.

The theory of Ref. 7 specifies that one should evaluate the nucleon-nucleon scattering amplitude $\langle \mathbf{p}' \mid T(p_0) \mid \mathbf{p} \rangle$ by summing the series in Fig. 1(a), where the box $\langle \mathbf{p}' \mid V(p_0) \mid \mathbf{p} \rangle$ includes various one-boson-exchange contributions to the quasipotential. The box is given diagrammatically in Fig. 1(b) and has the denominator structure

$$\langle \mathbf{p}' \mid V(p_0) \mid \mathbf{p} \rangle \sim (2E_{p_0} - E_p - E_{p'} - \omega_q)^{-1} (\omega_q)^{-1} \ , \tag{5}$$

where $E_p = (p^2+m^2)^{1/2}$ is the nucleon energy and $\omega_p = (p^2+\mu^2)^{1/2}$ is the meson energy corresponding to momentum $\mathbf{p}$. Because the quasipotential includes the meson retardation explicitly by virtue of the dependence on $E = 2E_{p_0}$ (the incident energy of the system), the box in Fig. 1 is drawn extended in time. The series in Fig. 1(a) is summed by the integral equation

$$\langle \mathbf{p}' \mid T(p_0) \mid \mathbf{p} \rangle = \langle \mathbf{p}' \mid V(p_0) \mid \mathbf{p} \rangle + \tfrac{1}{2} \int \frac{d^3p''}{(2\pi)^3} \frac{\langle \mathbf{p}' \mid V(p_0) \mid \mathbf{p}'' \rangle \langle \mathbf{p}'' \mid T(p_0) \mid \mathbf{p} \rangle}{E_{p_0} - E_{p''} + i\eta} \ . \tag{6}$$

It is the nature of this three-dimensional equation for T that a strict nonoverlap in time of the boxes in Fig. 1 is imposed on the sum. Contributions arising from overlapping boxes such as those shown in Fig. 2 arise in field theory and could be incorporated[9] in the model by adding terms to the definition of the quasipotential in Fig. 1(b).

In this paper we will use the folded-diagram method described in Refs. 4 and 5 to calculate a Hermitian, instantaneous potential corresponding to the selection of diagrams in Fig. 1. The method uses time-dependent perturbation theory and the resulting potential used in Eq. (2) gives the same $\langle \mathbf{p}' \mid T(p_0) \mid \mathbf{p} \rangle$ when $\mid \mathbf{p} \mid = \mid \mathbf{p}' \mid = p_0$. We evaluate the first two terms in the folded-diagram expansion for the potential; we expect this to be a reasonable procedure because the higher order terms are of progres-

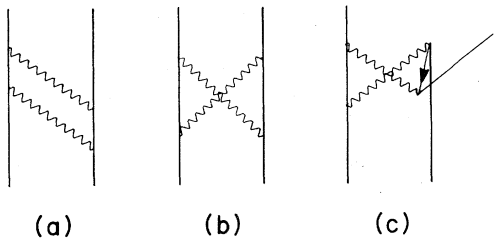

FIG. 2. Processes that contribute to the nucleon-nucleon potential in a field theory but that are omitted in the current investigation. The line pointing backward in time in (c) is an antinucleon state.

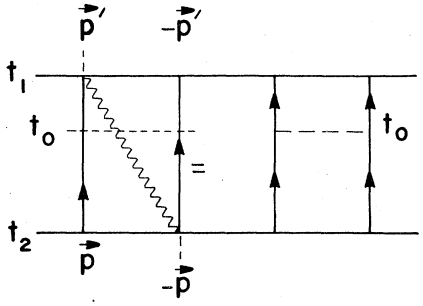

FIG. 3. The diagrammatic equation determining the instantaneous potential. To solve the equation, the external nucleon propagators must be removed from the right-hand side.

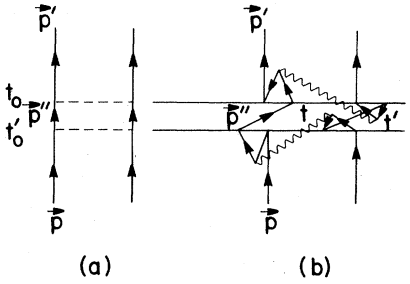

FIG. 5. Illustrating an unwanted time ordering of the potential $t > t'$.

sively shorter range and presumably less important at low energy.

To obtain the leading term we ask how the retarded one-meson exchange in Fig. 1(a) can be equated to an instantaneous potential. This clearly cannot be done exactly because there are two times characterizing Fig. 1(b), but only one time characterizing the instantaneous potential. Thus the equivalence can be established only in an average sense. The instantaneous potential is thus identified as an average over the extra time variable. In Ref. 5 it was shown how to do this time average diagrammatically. The equivalence is illustrated in Fig. 3. The time t_0 is the "time base" at which the potential acts. The solution of this equality is obtained by multiplying the left- and right-hand sides by the inverse of the propagator for the nucleons attaching to the potential. Each of the propagators corresponds to a time-dependent factor

$$[\exp(-iE_p\Delta t)] , \tag{7}$$

where E_p is the energy of a nucleon of momentum p where Δt is the time difference of the propagator line segment counted in the direction of the arrow on the line. The solution is expressed diagrammatically, as shown in Fig. 4. To get the complete potential, one must sum over the times t_1 and t_2 subject to the constraint that the potential acts at time t_0, where

$$t_0=\lambda_1 t_1+\lambda_2 t_2, \quad \lambda_1+\lambda_2=1 . \tag{8}$$

Results of the calculation and further discussion of the motivation is given in Ref. 5. A simple choice of t_0 is the average of t_1 and t_2, i.e.,

$$\lambda_1=\lambda_2=\tfrac{1}{2} . \tag{9}$$

We refer to this prescription as $J1$ below. Another possibility, $J2$, is

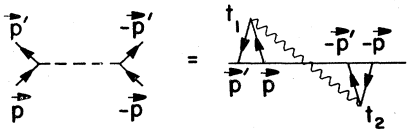

FIG. 4. The solution of the equation in Fig. 3.

$$\tfrac{1}{2}[(\lambda_1=0,\lambda_2=1)+(\lambda_2=0,\lambda_1=1)] . \tag{10}$$

Explicit expressions for the energy denominators in the center-of-mass system of the two nucleons are

$$(-q^2-\mu^2)^{-1} \tag{11}$$

for $J1$ and

$$(\Delta E^2-q^2-\mu^2)^{-1} \tag{12}$$

for $J2$, where

$$\Delta E\equiv\sqrt{p'^2+m^2}-\sqrt{p^2+m^2}$$

and $\mathbf{q}=\mathbf{p}'-\mathbf{p}$. The case $J1$ is the usual Yukawa potential and $J2$ is another form used in the literature.[10] We will also often make comparison to the non-Hermitian prescription of Ref. 6, which in our notation would correspond to

$$(\lambda_1=1,\lambda_2=0) . \tag{13}$$

We refer to this potential as K. It has the denominator structure

$$(-\Delta E-\omega_q)^{-1}(\omega_q)^{-1} . \tag{14}$$

The non-Hermiticity is evident from the fact that ΔE changes sign when the initial and final nucleon momenta are exchanged.

In second order the folded-diagram contributions to the instantaneous potential are obtained from the following considerations. We must ask to what extent the iteration of Fig. 4 reproduces the second-order piece of T given as the second term on the right-hand side of Fig. 1(a) with the box given in Fig. 1(b). Generally, the class of time or-

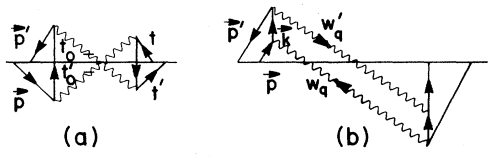

FIG. 6. Second-order fold diagrams. The horizontal lines on the mesons in (a) must maintain the time ordering $t_0 > t'_0$ because this is the time ordering of the potentials in Fig. 5(a). Likewise, $t > t'$.

derings generated by iterating the instantaneous potential and the quasipotential will be different. If there are extra time orderings generated by iterating the instantaneous potential, these must be subtracted by including a special term in the second-order potential. However, if there are fewer time orderings, these must be added as second-order corrections. It is easy to show after a bit of thought (see Ref. 5) that all relative time orderings of the second iteration of Fig. 1(b) are generated by the second iteration of Fig. 4. However, the second iteration of Fig. 4 produces several unwanted terms.

The unwanted time orderings can be found for the prescription $J1$ by substituting Fig. 4 into Fig. 5(a). When $t > t'$, which must sometimes occur because of the average performed in the definition of the one-meson-exchange potential in Fig. 4, one such term arises. It may be converted to a contribution in the instantaneous potential by picking a time base and folding the external legs back to it as in Fig. 4. The simplest choice of time base is the average of the four times at the vertices in Fig. 5(b). The appearance of the diagram may be simplified by straightening out the lines on the right-hand side of Fig. 5(b), which is permissible because of the exponential form of the propagator in Eq. (7). The result is shown in Fig. 6(a). Figure 6(b) is another time ordering that is included when Fig. 4 is iterated. This is the same as Fig. 2(a), and it is interesting to see that the folded-diagram potential automatically includes the stretched-box diagrams that must be added explicitly in the theory of Ref. 9. However, the model exact results in the present paper do not include the stretched box diagrams. Therefore, both terms in Fig. 6 occur in the potential with a minus sign because they represent time orderings that must be removed.

The rules for evaluating the terms in Fig. 6 are discussed in Ref. 5. The results of applying these rules lead to the following denominator structure[11] for Fig. 6(a):

$$-\frac{1}{2}\frac{1}{\bar{E}-E_k-\omega_q'}\left[\frac{\bar{E}-E_k-\omega_q'-\omega_q}{\omega_q'\omega_q}+\frac{1}{\omega_q'+\omega_q}\right]\frac{1}{\bar{E}-E_k-\omega_q}, \quad (15)$$

where $\bar{E}=\frac{1}{2}(E_p'+E_p)$. It turns out that the second term in the parentheses is numerically equal to (minus) the diagram in Fig. 6(b), and subtracting Fig. 6(b) means eliminating this term. We do not consider the second-order corrections for $J2$ in this paper.

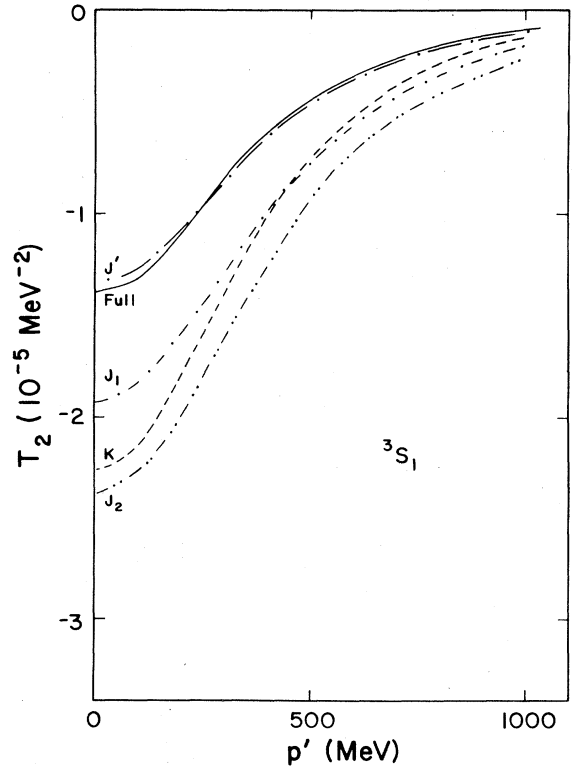

FIG. 7. Real part of the second Born approximation to the T matrix for pions only. The solid curve is the model-exact result. The one-pion-exchange potential results are the following: short-dashed/double-dot curve, $J2$ prescription [Eq. (10)]; short-dashed curve, K prescription [Eq. (13)]; and short-dashed/dot curve, $J1$ prescription [Eq. (9)]. The long-dashed/dot curve includes the second-order fold for the $J1$ prescription.

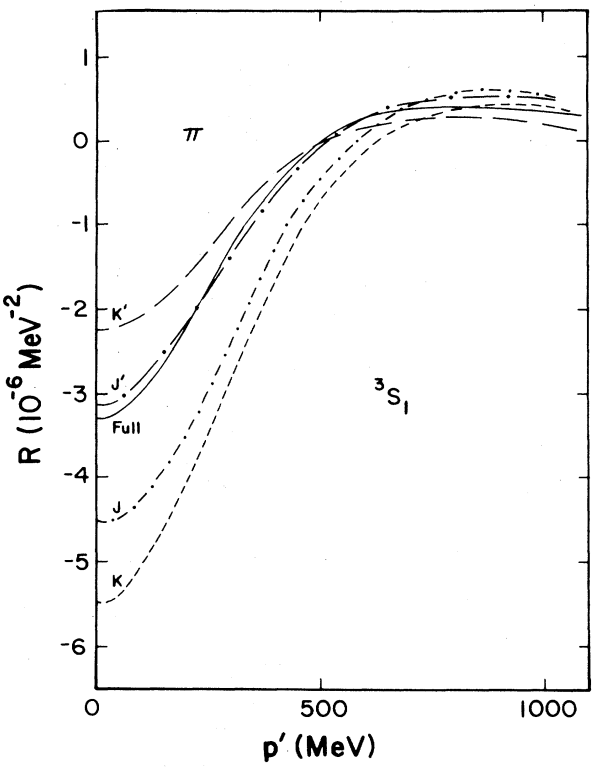

FIG. 8. The R matrix for pions only. The solid curve is the model-exact result. The one-pion-exchange potential results are the following: short-dashed curve, non-Hermitian K prescription [Eq. (13)]; and short-dashed/dot curve, Hermitian J prescription [Eq. (9)]. The one-pion plus two-pion folded-diagram result are the following: long-dashed curve, non-Hermitian result; long-dashed/dot curve, Hermitian result.

III. RESULTS

To indicate the importance of the folded diagrams, we show in Fig. 7 the various contributions to the second Born approximation of the T matrix in Eq. (6) for $|\mathbf{q}| = q_0 = 250$ MeV/c. The solid line is our model-exact results, assuming pions only as the meson exchanged in the box in Fig. 1(a). The short dot-dashed curve is the iteration of the folded-diagram potential of Fig. 4, corresponding to the $J1$ choice [see Eqs. (9) and (11)]. The short double-dot/dashed curve corresponds to $J2$ [see Eqs. (10) and (12)]. The K choice [see Eqs. (13) and (14)] is the short-dashed curve.

The three one-meson-exchange potentials give different results from each other and the model-exact result because of the different treatments of meson retardation. When the two-meson-exchange folded diagrams are added, we expect the agreement to improve. In fact, for the non-Hermitian case the agreement is exact for the half-off-shell matrix elements; the non-Hermitian potential is defined so that the half-off-shell second Born approximation is the same in the two cases. The result of adding the two-meson-exchange folded diagram corresponding to the $J1$ prescription is shown as the dot/long-dashed curve. It coincides with the solid curve for the on-shell matrix element as it should according to the definition of the second-order potential. It is interesting to see how closely the solid and dot/long-dashed curves coincide for the off-shell points. For the fully off-shell matrix elements, the Hermitian, non-Hermitian, and model-exact matrix elements would all differ. We hasten to remind the reader that the relevant criterion is how well the phase shifts, or on-shell values of the full T matrix, agree in the various cases. We examine this shortly.

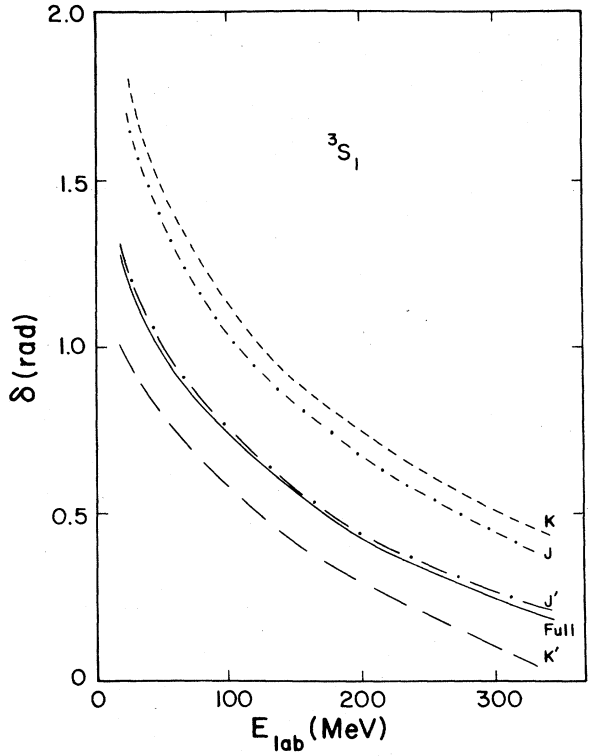

FIG. 10. Phase shift for the $^3S_1$ channel, pions only. The legend is the same as Fig. 8.

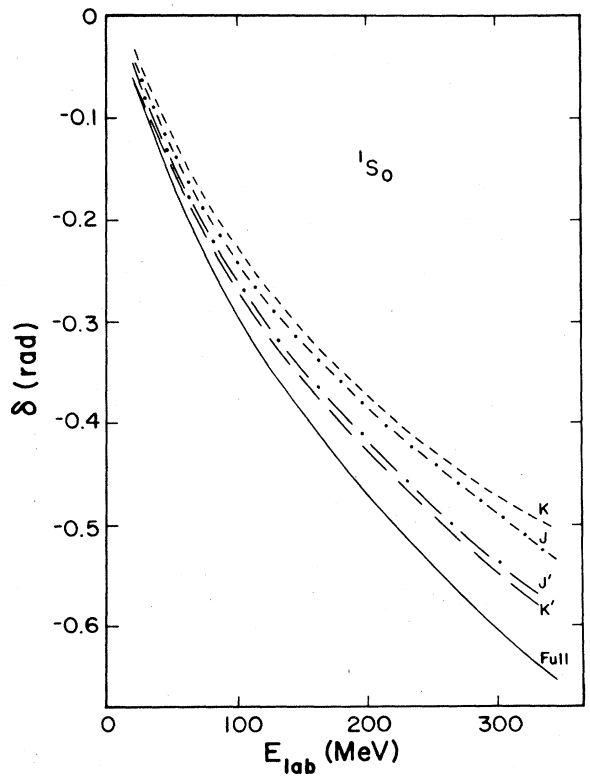

FIG. 9. Phase shift for the $^1S_0$ channel, pions only. The legend is the same as Fig. 8.

We can understand the relative sizes of the $J1$, $J2$, and K one-meson approximations in Fig. 7 in the following way. Note that the $J2$ prescription is further away from the exact result than either $J1$ or K. This is generally true in our calculations and it can be understood analytically by comparing Eq. (5) (model exact), Eq. (11) ($J1$ prescription), and Eq. (12) ($J2$ prescription). Note that the correction to $-\omega_q$ in Eq. (5) is negative. (It is the nature of the meson-nucleon coupling that large values of $\langle \mathbf{p} \rangle$ and $\langle \mathbf{p}' \rangle$ are important so that for the energies considered, $q_0 < \langle \mathbf{p} \rangle$ and $q_0 < \langle \mathbf{p}' \rangle$.) However, for $J2$ the ΔE^2 correction to $-\omega_q^2$ in Eq. (12) is positive. Thus the $J2$ potential is generally *larger* than the model-exact result. The $J1$ potential is intermediate in size because it has no correction term. The sign of the correction term in the non-Hermitian results of Eq. (14) is not positive definite, so it would be expected to be similar to the $J1$ result; one sees in Fig. 7 that whether or not $J1$ or K is closer to the model-exact result depends on the incident energy.

Earlier, in Ref. 5, a formal reason for preferring $J1$ was given, namely that it required fewer folded-diagram corrections than the $J2$ prescription suggesting a better rate of convergence for $J1$. Now we have seen that $J1$ is better than $J2$ by comparing the numerical results. In the remaining comparisons of this paper we show results for the Hermitian prescription $J1$ only and refer to it as J.

The magnitude of all terms in T_2 of Fig. 7 is very sensitive to the vertex cutoff $V(k)$ in the pion-nucleon coupling,

$$V(k)=\frac{\Lambda^2-m^2}{k^2+\Lambda^2}\ , \tag{16}$$

where m is the mass of the pion and Λ is the vertex cutoff. The value of Λ in Fig. 7 is 2000 MeV. If we reduce it to $\Lambda=1000$ MeV, the magnitude of the different curves is decreased by about 60% at small q', but otherwise the results are very similar. In our subsequent calculations we use Λ as it comes from the one-boson-exchange model of Ref. 7, which for pions is $\Lambda_\pi=1500$ MeV.

Let us now look at the complete scattering amplitude. This is a complex quantity, so we simplify the discussion by examining its real part, the R matrix. We show this in Fig. 8 for the same half-off-shell kinematics as Fig. 7, i.e., $|\mathbf{q}|=q_0=250$ MeV/c. As in Fig. 7, the J and K lowest order approximations undershoot the model-exact result at small q, but they cross over the exact result at large q. The addition of two-meson-exchange folds, giving the results J' for the Hermitian and K' for the non-Hermitian cases, repairs much of the discrepancy. For the $^3S_1$ case shown here, J' is a better approximation than K', but in other channels the K' result is sometimes better. Note that K' is no longer equal to the model-exact result, even though the R matrix is half on shell.

Next consider the calculation of the phase shifts for the

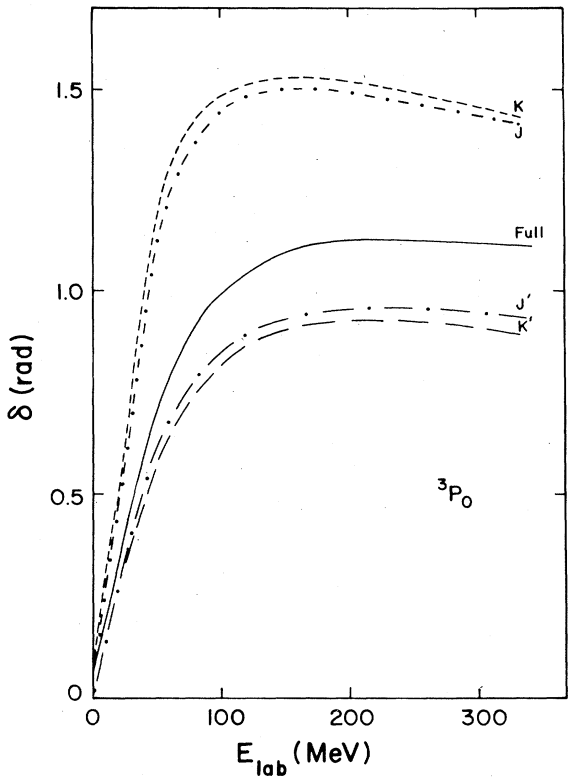

FIG. 12. Phase shift for the $^3P_0$ channel, pions only. The legend is the same as Fig. 8.

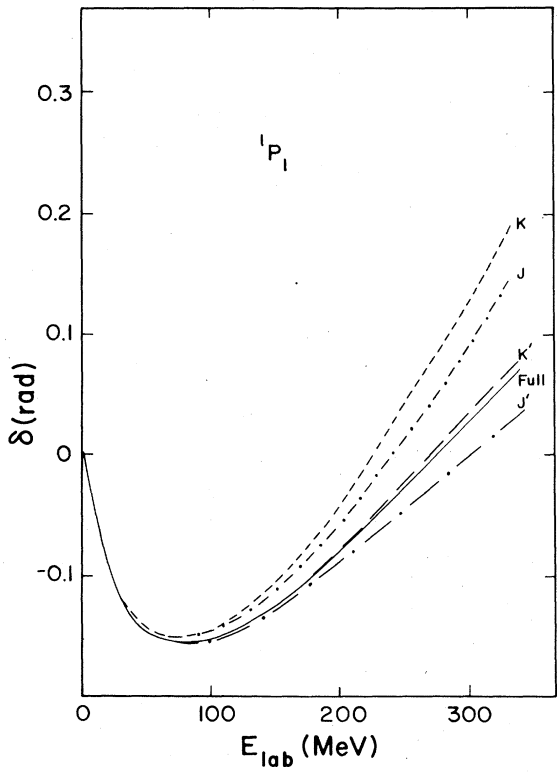

FIG. 11. Phase shift for the $^1P_1$ channel, pions only. The legend is the same as Fig. 8.

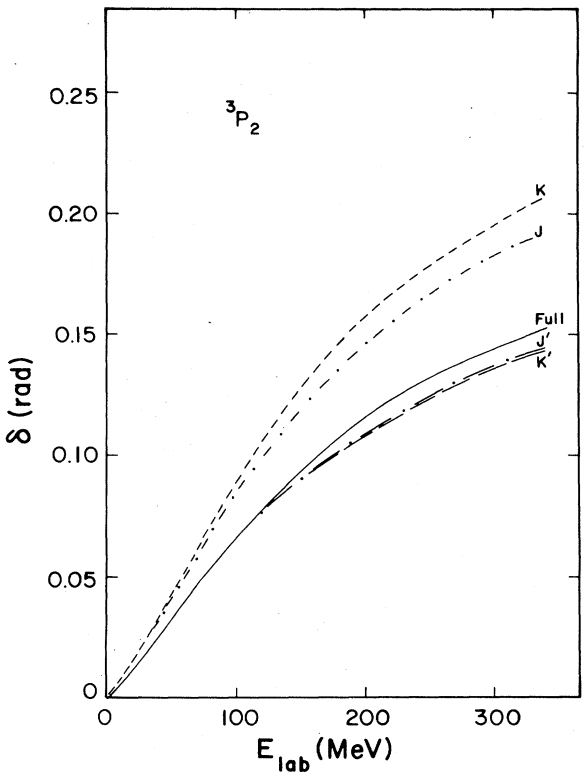

FIG. 13. Phase shift for the $^3P_2$ channel, pions only. The legend is the same as Fig. 8.

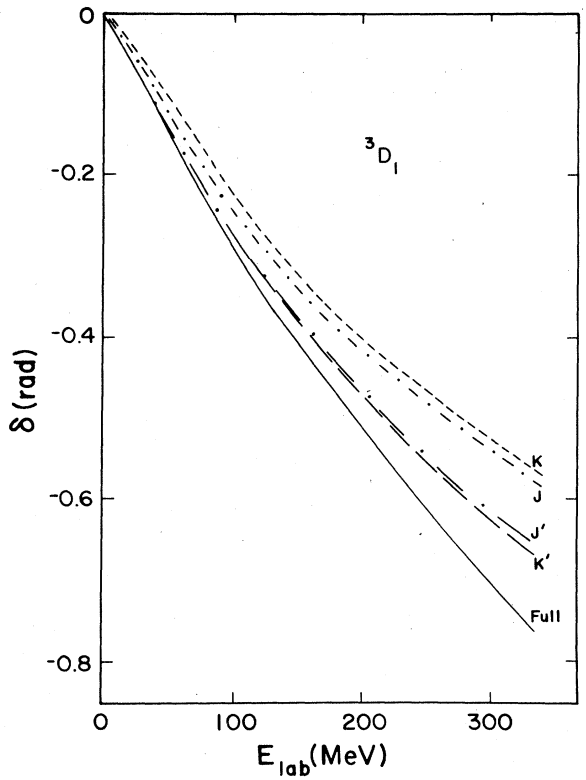

FIG. 14. Phase shift for the $^3D_1$ channel, pions only. The legend is the same as Fig. 8.

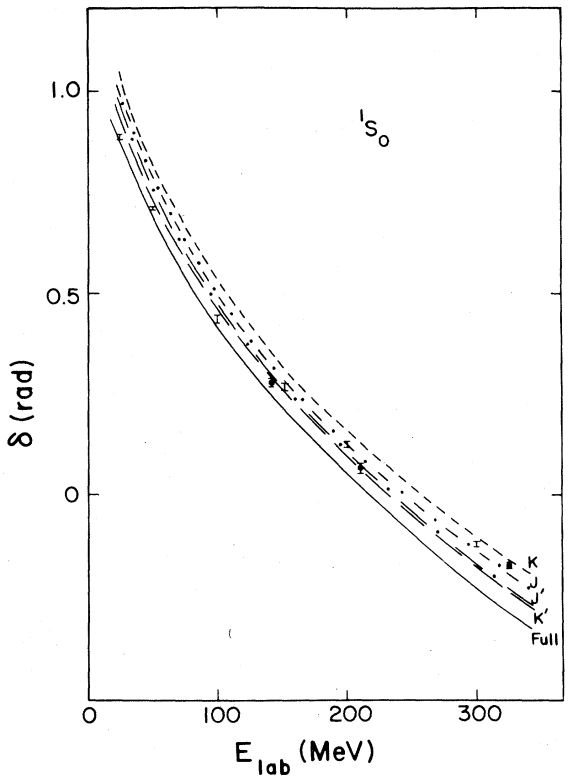

FIG. 16. Phase shift for the $^1S_0$ channel, full OBEP. The legend is the same as Fig. 8. The experimental phase shifts are from Ref. 12 (Ŧ) and Ref. 13 (I).

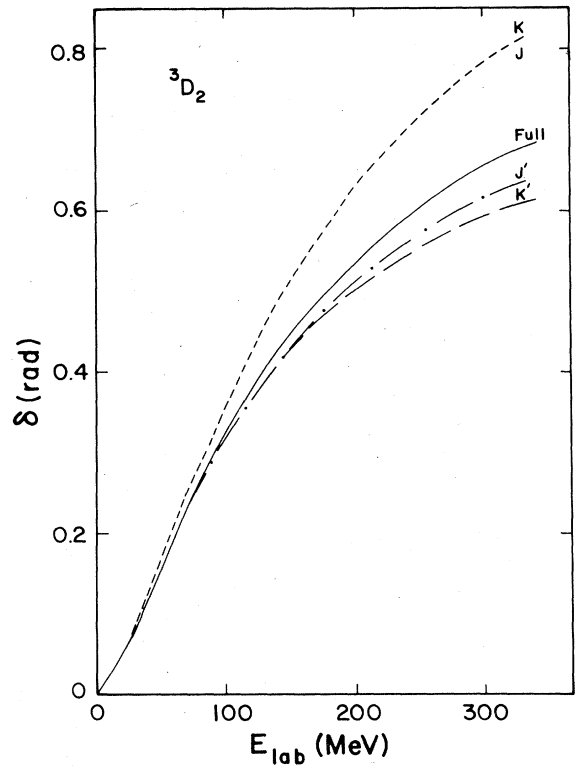

FIG. 15. Phase shift for the $^3D_2$ channel, pions only. The legend is the same as Fig. 8.

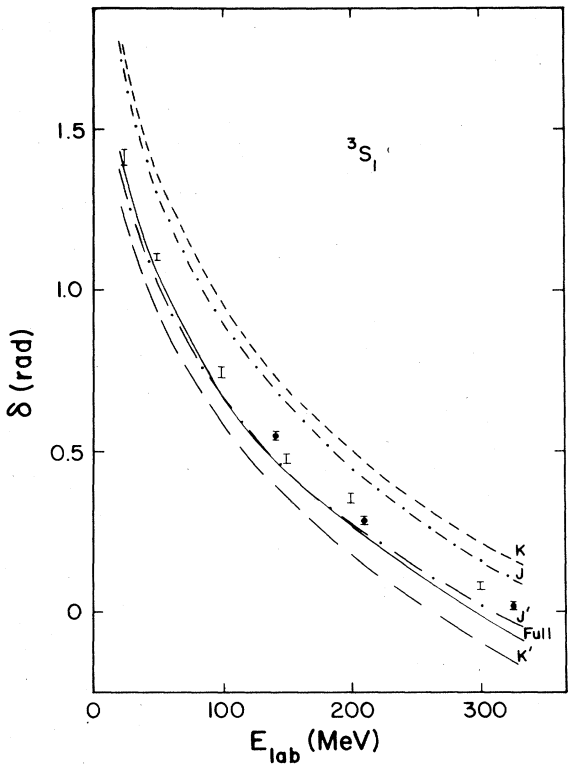

FIG. 17. Phase shift for the $^3S_1$ channel, full OBEP. The legend is the same as Fig. 16.

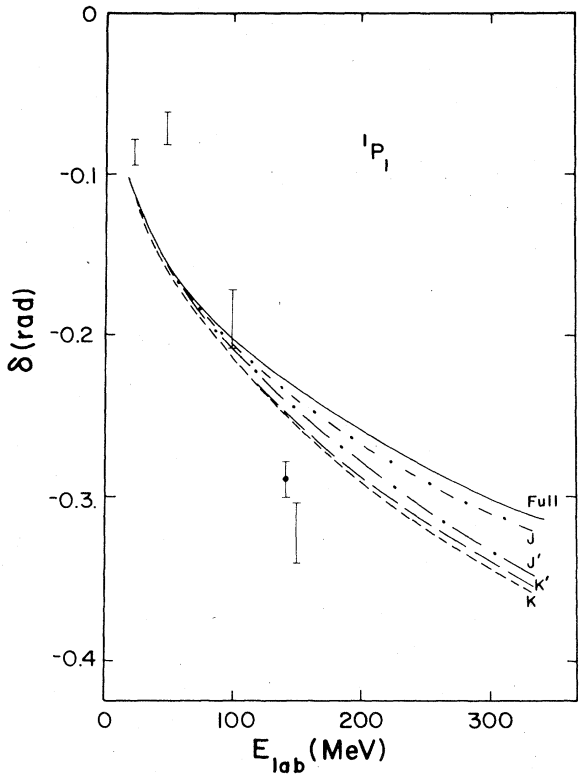

FIG. 18. Phase shift for the $^1P_1$ channel, full OBEP. The legend is the same as Fig. 16.

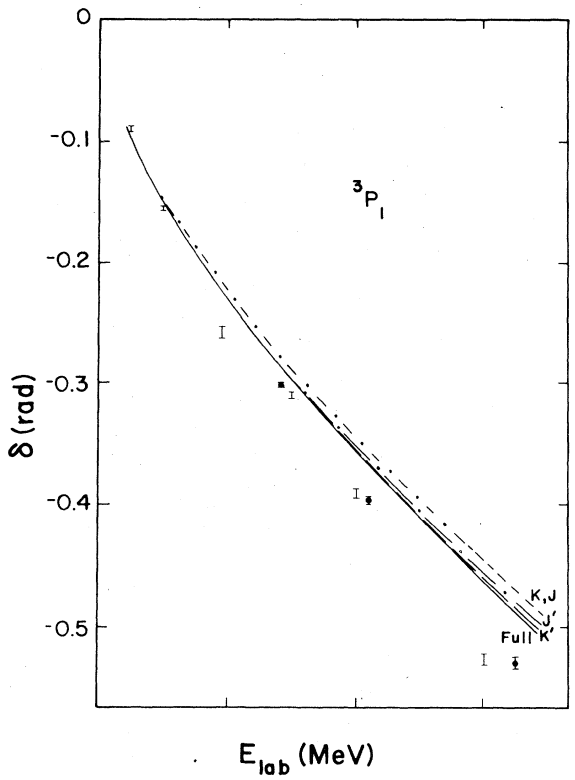

FIG. 20. Phase shift for the $^3P_1$ channel, full OBEP. The legend is the same as Fig. 16.

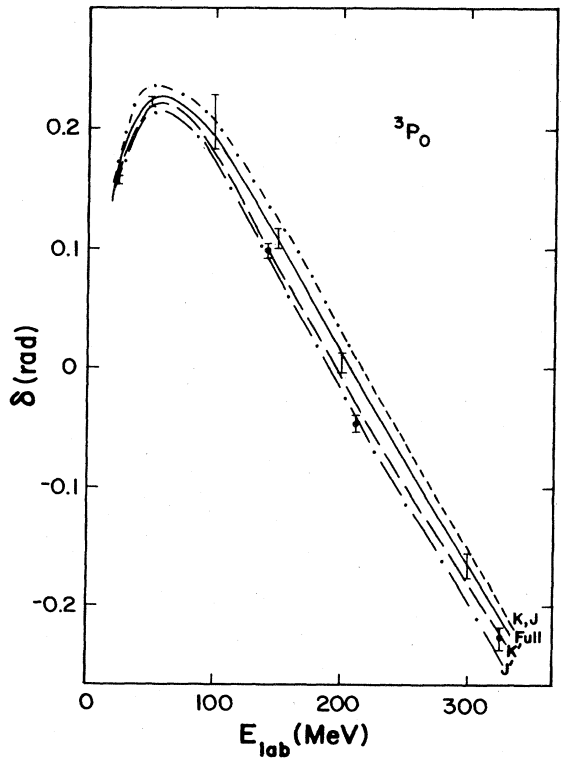

FIG. 19. Phase shift for the $^3P_0$ channel, full OBEP. The legend is the same as Fig. 16.

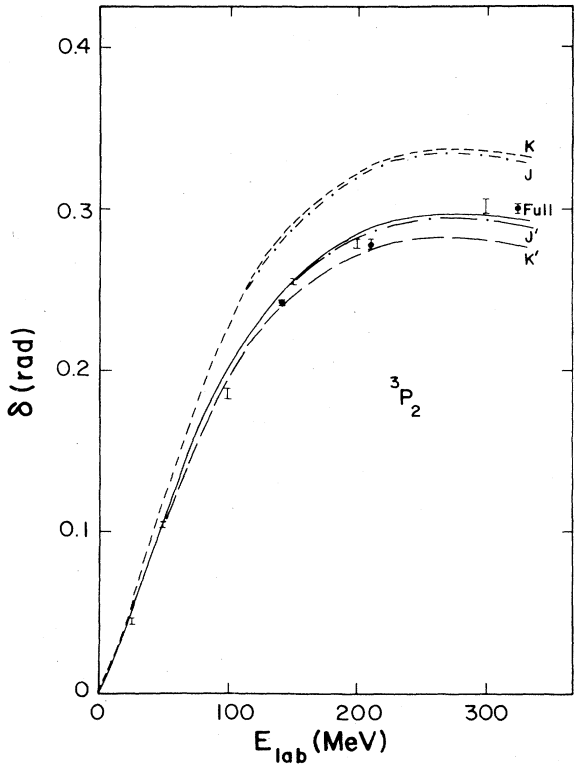

FIG. 21. Phase shift for the $^3P_2$ channel, full OBEP. The legend is the same as Fig. 16.

case of pion exchange. Figures 9—15 compare the J and K prescriptions in this case. It is interesting to see that the lowest order Hermitian potential is always closer than the non-Hermitian result. One might expect from this result that when the second-order folded diagram is added, the Hermitian result would also be closer. This is often the case, for example, in the channels $^3S_1$, $^3P_0$, $^3P_2$, and $^3D_2$, but not in $^1S_0$, $^1P_1$, and $^3D_1$. In the latter cases, the differences between J' and K' are either small or, as in $^1P_1$, the phase shift is close to zero, where the fractional differences are large. For the higher partial waves the Hermitian and non-Hermitian results are essentially in agreement with the model-exact result.

Next consider the OBEP potential. In second order we consider only the folded diagrams involving two pions because this contribution is of longer range than those involving heavier mesons and presumably the most important one. The OBEP is a rather different case from the one-pion exchange because of the strong repulsion at short distances arising from ω-meson exchange. One might expect that the correlations arising from the repulsion would diminish the importance of the folded diagrams, which are intrinsically of shorter range and therefore make the Hermitian and non-Hermitian prescriptions look more similar. However, because we omit the second-order folds involving heavier mesons, such expectation may not be realized. Figures 16—24 show the results for the OBEP. We see that the lowest order Hermitian potential is at least as close to the model-exact result as the non-

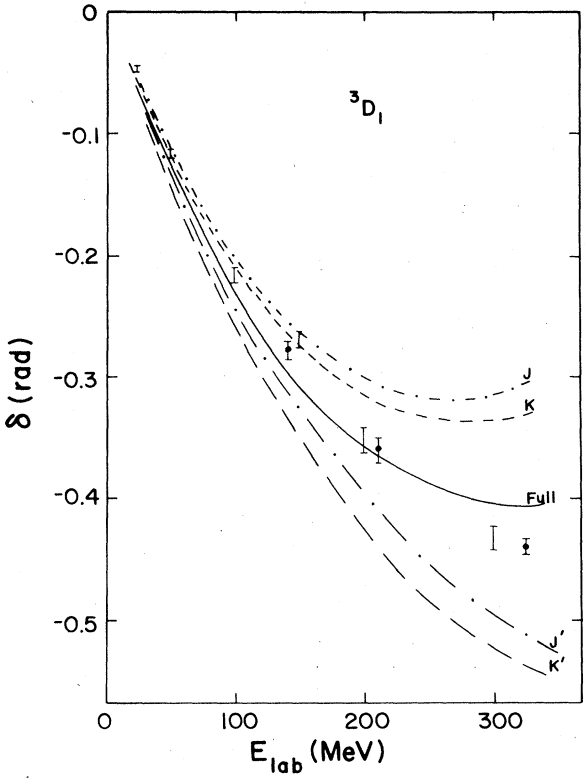

FIG. 23. Phase shift for the $^3D_1$ channel, full OBEP. The legend is the same as Fig. 16.

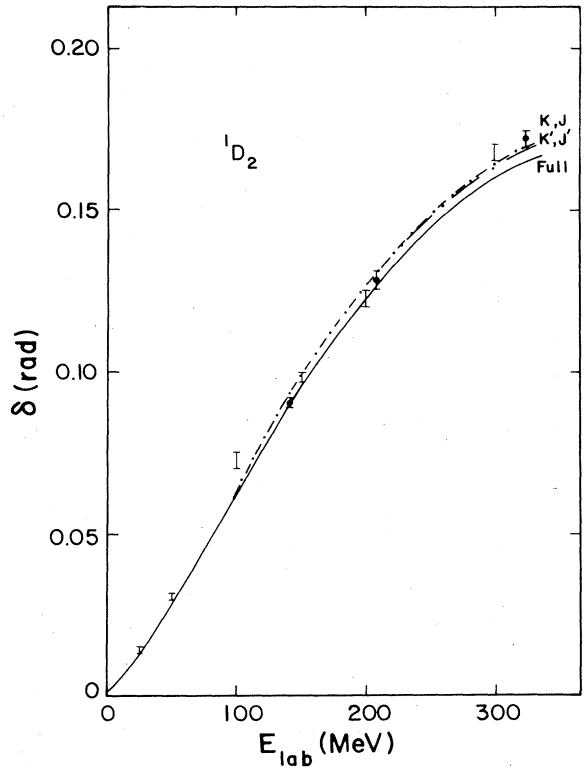

FIG. 22. Phase shift for the $^1D_2$ channel, full OBEP. The legend is the same as Fig. 16.

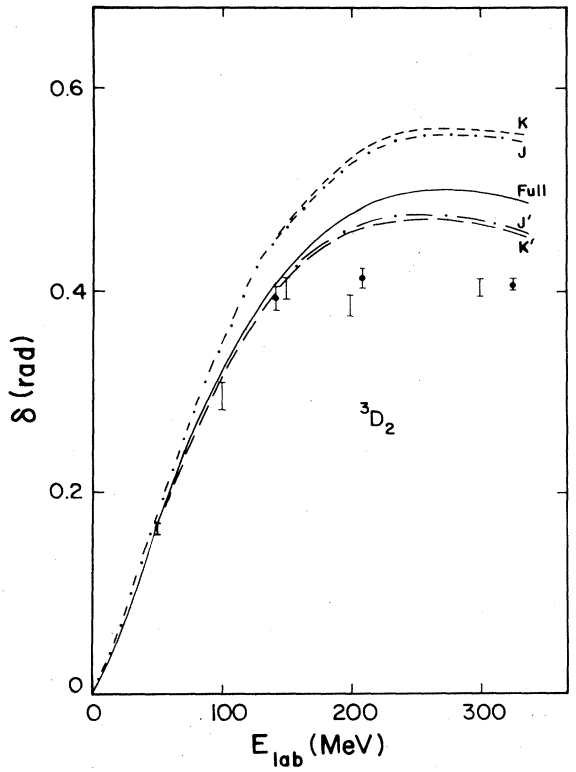

FIG. 24. Phase shift for the $^3D_2$ channel, full OBEP. The legend is the same as Fig. 16.

Hermitian potential in all cases but $^3D_1$. When the folded diagram is added, this continues to be the case in the channels $^3S_1$, $^1P_1$, $^3P_2$, $^1D_2$, $^3D_1$, and $^3D_2$. The non-Hermitian result is slightly closer to the model-exact result for the cases $^1S_0$, $^3P_0$, and $^3P_1$.

The rate of convergence of the folded-diagram expansion appears to be quite favorable in the cases shown. The discrepancies with the model-exact result are on the order of 10% except for $^3D_1$, where they are 20—25 % at the higher energies. The discrepancies were smaller in the one-pion-exchange potential (OPEP) case for $^3D_1$, suggesting that the large differences in OBEP may be due to the omission of folds involving the heavier mesons.

IV. DISCUSSION AND CONCLUSIONS

The basic question being addressed here is whether a Hermitian, energy-independent potential is an adequate basis for the description of the nucleon-nucleon interaction. One might believe that the interaction requires energy dependence to account for the retardation of meson exchange. The Bethe-Salpeter kernel, the Bonn potential, and original form of Paris potential are examples of interactions that are more complicated, with explicit energy dependence. In this paper we have shown that the folded-diagram potential, including terms through two-meson exchange, gives an on-shell scattering amplitude very close to that of the one-boson-exchange (OBE) version of the Bonn potential.

Because there exist many expansions leading to instantaneous potentials, the question of which one to choose in practice is of great interest. We have looked at three. Two expansions discussed in Ref. 5 lead to Hermitian potentials and the one of Ref. 9 leads to a non-Hermitian potential. We found that of the two Hermitian potentials, the prescription $J1$ gave the best results without the fold and concluded that it corresponds to the most rapidly convergent prescription. The OBEP in this case closely resembles the usual Yukawa interaction.

In comparing the case $J1$ with the non-Hermitian potential, we found that the $J1$ is almost always better than the non-Hermitian potential at the level of one-meson exchange, but that when the single folds are added, the two are nearly equivalent. We conclude that on the basis of the on-shell comparisons, there is no practical advantage of using non-Hermitian folded-diagram prescriptions.

Finally, we checked the extent to which the half-off-shell T matrix is reproduced in the Hermitian and non-Hermitian prescriptions. We found that even though the non-Hermitian potential was invented to preserve this property in principle, in practice it is not easy to accomplish. In fact, in the case we chose to examine, the Hermitian potential gave a superior reproduction of the off-shell amplitude.

We need folded diagrams to achieve agreement with the OBE model of the Bonn potential. This might be considered a complication. However, in more sophisticated models two-meson-exchange contributions are required and at this level the method of folded diagrams is no more complicated than calculating T with the energy-dependent formalism.

The numerical results presented here are only a partial answer to the question of whether the Hermitian or non-Hermitian potential is the most adequate description. We have found that for the purpose of calculating phase shifts the two are roughly equivalent. However, it may be the case that studies of effective operators would lead to a different conclusion. Effective operators are required if one wants to calculate quantities that probe off-shell properties of the interaction. In any case, meson retardation effects in observables such as electron-scattering form factors and magnetic moments have not been sufficiently carefully investigated in the past, and we believe that a study of observables paralleling that given here for the potential would be interesting.

ACKNOWLEDGMENTS

One of the authors (K. H.) wants to thank the staff of LAMPF for the kind hospitality extended to him during his stay at Los Alamos. This work was supported in part by Deutsche Forschungsgemeinschaft.

---

*Permanent address: Institut für Theoretische Kernphysik der Universität Bonn, Nussallee 14-16, D-5300, Bonn, Federal Republic of Germany.

[1]B. H. Brandow, Rev. Mod. Phys. **39**, 771 (1967); in *Lectures in Theoretical Physics,* edited by K. T. Mahanthappa (Gordon and Breach, New York, 1969), Vol. II.

[2]G. Oberlechner, F. Owono-N'-Guema, and J. Richert, Nuovo Cimento **B68**, 23 (1970).

[3]T. T. S. Kuo, S. Y. Lee, and K. F. Ratcliff, Nucl. Phys. **A176**, 65 (1971).

[4]M. B. Johnson and M. Baranger, Ann. Phys. (N. Y.) **62**, 172 (1971).

[5]M. B. Johnson, Ann. Phys. (N. Y.) **97**, 400 (1975).

[6]G.-L. Li, K. K. Ng, and T. T. S. Kuo, Phys. Rev. C **25**, 2877 (1982).

[7]Updated version of K. Kotthoff, K. Holinde, R. Machleidt, and D. Schütte, Nucl. Phys. **A242**, 429 (1975).

[8]G. DeGuzman, T. T. S. Kuo, K. Holinde, R. Machleidt, A. Faessler, and H. Müther, Nucl. Phys. (to be published).

[9]R. Machleidt, *Lecture Notes in Physics* (Springer, Berlin, 1984), Vol. 197, p. 352.

[10]K. Erkelenz, Phys. Rev. C **13**, 191 (1974); N. Fukuda, K. Sawada, and M. Taketani, Prog. Theor. Phys. **12**, 156 (1954).

[11]There is a mistake in Eqs. (49)—(51) of Ref. 5. The function $\theta(t_2'-t_2)$ in Eq. (49) should be $\theta(t_2-t_2')$. The results in Eq. (15) of this work have taken account of the correction.

[12]R. Dubois, D. Axen, R. Keeler, M. Comyn, G. A. Ludgate, J. R. Richardson, N. M. Stewart, A. S. Clough, D. V. Bugg, and J. A. Edington, Nucl. Phys. **A377**, 554 (1982).

[13]R. A. Arndt, L. D. Roper, R. A. Bryan, R. B. Clark, B. J. VerWest, and P. Signell, Phys. Rev. D **28**, 97 (1983).